LIP-STUDENTS-25-24

Measurement of the muon flux at the LHC using the sRPC detector

João Goulão[1,a] and Rafael Fernandes[1,b]

[1] *Instituto Superior Técnico*

Project supervisor: Cristóvão Vilela and Nuno Leonardo

November 27, 2025

Abstract. The sRPC detector is a supplementary detector for the SND@LHC experiment. It is a sealed Resistive Plate Chamber detector, which presents advantages over standard RPC detectors in operation reliability and environmental impact due to its ability to operate without gas flow. The detector was installed with the main purpose of calculating the flux of the important muon background created at the ATLAS experiment, so as to improve detection of neutrinos at SND@LHC. We have utilized data from a run of the LHC to obtain the muon flux, which is found to be 1.01×10^5 for an area of 30×21 cm^2, and 6.39×10^4 for an area of 30×30 cm^2. We have also utilized a Monte Carlo simulation as a model for the flux, obtaining deviations from the real result between 60% and 120%, and concluding that the simulated flux values were overestimated.

Keywords: SND@LHC, muon flux, RPC

1 Introduction

1.1 The sRPC detector

The SND@LHC is an ongoing experiment at the Large Hadron Collider (LHC) whose purpose is to detect and measure neutrinos produced in proton-proton collisions. As a part of the SND@LHC experiment, a secondary detector, named sRPC (sealed Resistive Plate Chamber), designed and built at LIP, was installed at the SND@LHC site and has been operational since 2023. In contrast to standard RPCs, the sRPC does not require a flowing gas, which eliminates various practical and environmental issues.

Figure 1: sRPC detector

The detector was installed upstream of the SND@LHC, approximately 480 metres away from the ATLAS collision point. Its main goal is to measure the muon flux, which constitutes a dominant part of the background in neutrino detection. This will be complimentary to a similar measurement previously made for the SND@LHC detector.

[a] e-mail: joao.goulao@tecnico.ulisboa.pt

[b] e-mail: rafael.a.fernandes@tecnico.ulisboa.pt

The sRPC system comprises four detector 30x30 cm planes, equally separated by 17 cm. Each plane is segmented into 16 parallel strips that can acquire data from both ends (front and back). Each strip is able to measure the induced charge (QB and QF) and the time of arrival of the signal at each end (TB and TF), enabling precise reconstruction of the particle's trajectory. With the collected data, the position can be reconstructed as follows:

- $x = \frac{TF-TB}{2} \times v$, where v is the signal propagation velocity along the strip (165.5 mm/ns).
- y = strip position corresponding to the maximum collected charge.
- z = plane position.

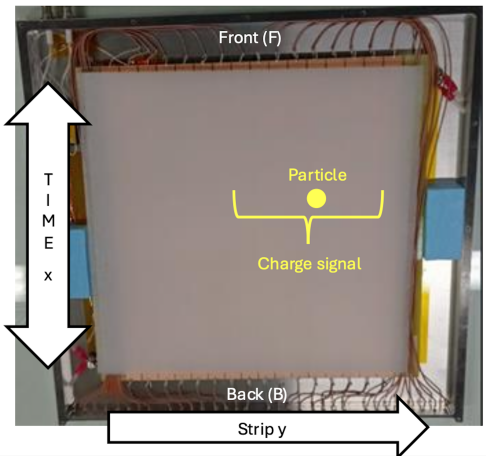

Figure 2: Coordinate system of the sRPC detector

1.2 Monte Carlo simulation

When the muon flux was calculated for the SND@LHC detector, a Monte Carlo simulation was utilized as a prediction method.[1] This simulation was structured into three phases: the production of muons at the ATLAS detector through proton-proton collisions; the propagation of

those particles to the SND@LHC site and muon production by particle decay in the course of such propagation; and propagation and interaction through the SND@LHC detector.

For our study, we utilized a version of this simulation apparatus. The simulated data analyzed was taken from the end of the second phase, so as to not get interference in the data from the SND@LHC detector itself, which is separate from the sRPC detector. This decision has implications in the results of the flux, as the last phase of the simulation contains some material between the end of phase two and the surface of our detector.

The data produced by the simulation contains several events, with parameters that allow for their characterization. Among those parameters, we were interested in studying position (in x and y coordinates), particle id (according to [2]), and weight.

The data points are hence distributed in a scoring plane of 180x180cm^2, which ranges in coordinates from -90 to 90 in both x and y. All received particles are either muons, with id = 13, or antimuons, with id = -13.

The weight of each event, although not having any significance by itself, allows for the direct calculation of the flux.

2 Detector Data Analysis

Using the coordinates defined in section 1.1, we can construct a hit map. As an example, the hit map of the first plane is shown in fig. 3.

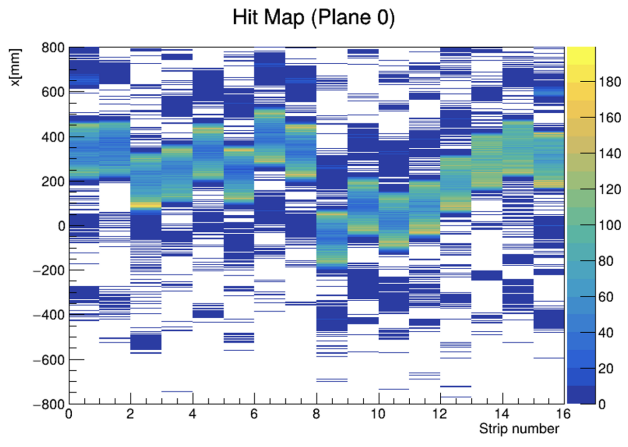

Figure 3: First plane hit map without calibration

As observed, the distribution is very dispersed, indicating the need for a calibration in order to visualize and analyze the data clearly.

2.1 Calibration

2.1.1 Time Calibration

To perform the time calibration and determine the time offset, we analyze the histogram of the time differences and set a threshold at half the histogram's maximum height. The first (P1) and last (P2) intersection points are calculated and their average computed. The midpoint is taken as the time offset:

$$T_{\text{offset},i,p} = \frac{P1 + P2}{2} \tag{1}$$

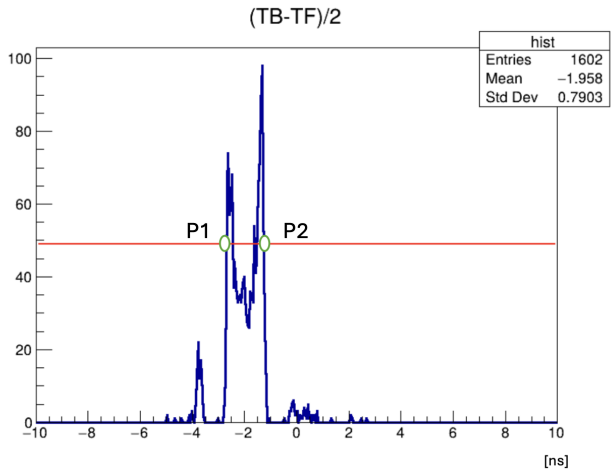

Figure 4: Time difference plot

2.1.2 Charge Calibration

For the charge calibration, the QB or QF histograms are analyzed (fig. 5). Then the cumulative density function (CDF) is calculated and compared to a linear function (fig. 6). The point at which the distance between the CDF and the linear function is maximum is taken as the charge offset.

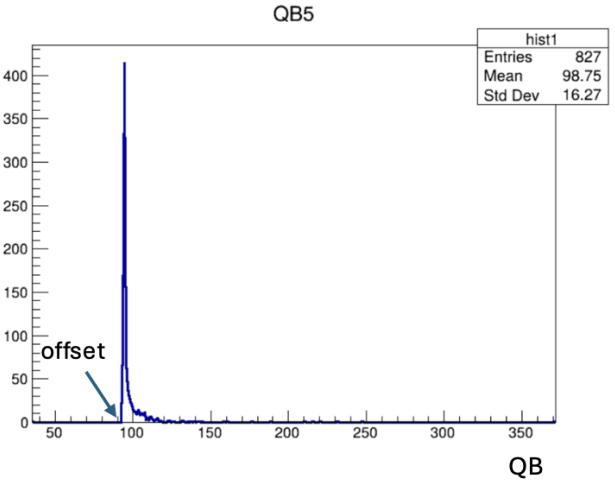

Figure 5: Histogram of QB from strip five of plane 0.

2.1.3 Calibrated Hit Maps

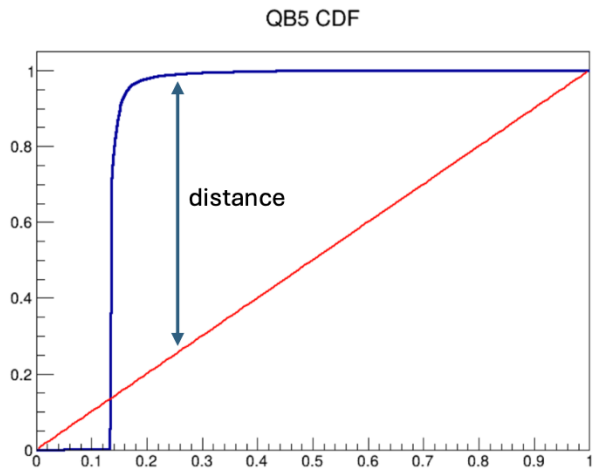

Figure 6: Comparison between CDF of QB from strip five of plane 0 and linear function.

With the offsets calculated, we can calibrate the data as:

$$Q_{\text{calibrated},i,p} = Q_{\text{measured},i,p} - Q_{\text{offset},i,p} \quad (2)$$

$$T_{\text{calibrated},i,p} = \frac{T_{F,\text{measured},i,p} - T_{B,\text{measured},i,p}}{2} - T_{\text{offset},i,p} \quad (3)$$

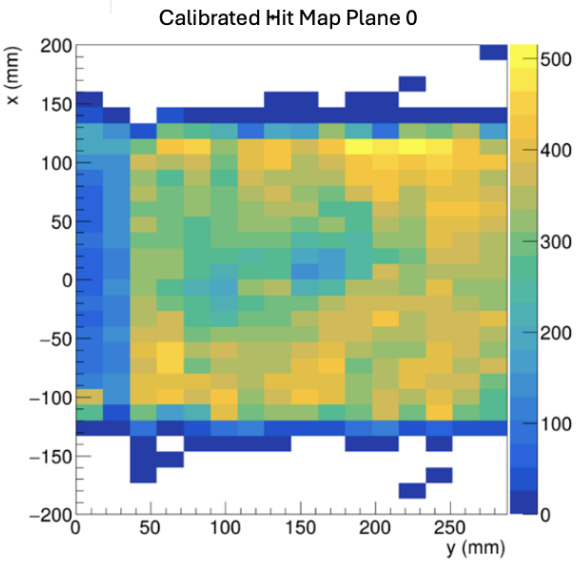

Figure 7: Calibrated hit map of plane 0

With the calibration completed, we can now proceed with the data analysis.

2.2 Reconstructed Trajectories

In order to describe the trajectory of the particles passing through the detector, two types of plots were produced: strip number vs. plane number and time difference vs. plane number.

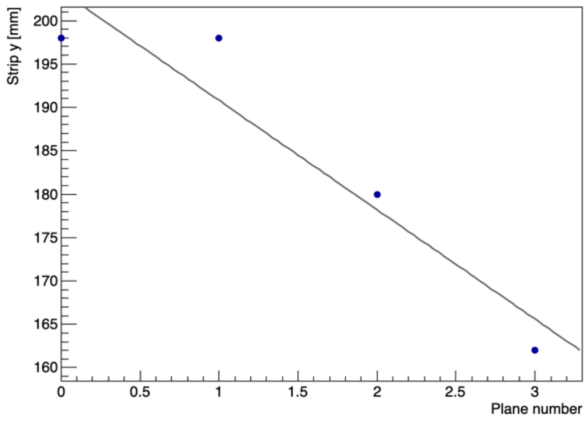

Figure 8: Strip number vs plane number of an event.

The selection criterion for valid events was the presence of three hits in at least three different planes. In cases with only three hits, a linear function was fitted to estimate the position of the missing hit.

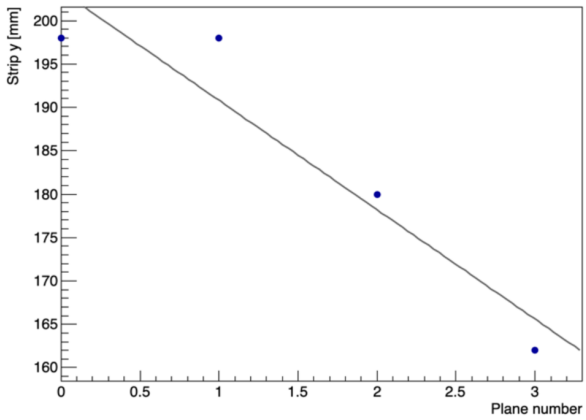

Figure 9: Strip number vs plane number of an event.

2.3 Efficiency

The reconstructed trajectories were used to calculate the efficiency of each detector plane. It is important to note that the efficiency is not constant throughout the entire area of the detector, as shown in fig.10.

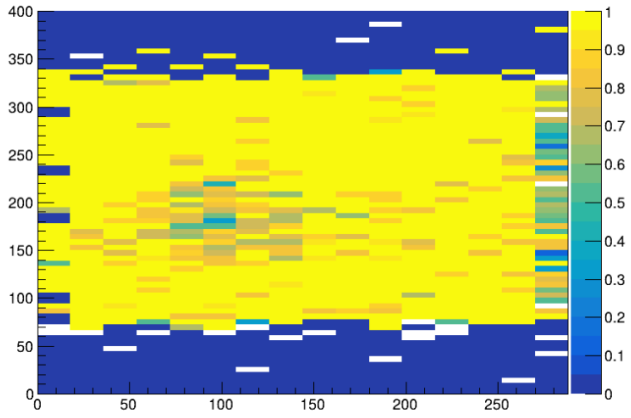

Figure 10: Efficiency map of plane 0.

A calculation of the overall efficiency for each plane was made; the results are presented in the following table.

Table 1: Efficiency for the different planes

Plane	0	1	2	3
Efficiency	76.8%	97.3%	98.2%	74.5%

It is easy to notice that the first and last plane have lower efficiency than the ones in the middle. This is due to the fact that the sRPC detector is tilted in relation to the incoming particle flux. As a result, the probability of recording a hit in the outer planes is smaller compared to the middle ones.

The overall efficiency of the detector was calculated using the following formula.

$$\varepsilon_{\text{total}} = \sum_{1\le i<j<k\le 4} \varepsilon_i \, \varepsilon_j \, \varepsilon_k - 3 \prod_{i=1}^{4} \varepsilon_i \tag{4}$$

This gave us the following value for the detector efficiency: 92.0%.

To mitigate the effects of the tilted detector, the same calculations were made using an area where all planes had coverage and the simulation had data for direct comparison (30x21cm^2). The resulting values are summarized in table 2.

Table 2: Efficiency for the different planes (reduced area)

Plane	0	1	2	3	Total
Efficiency	71.3%	92.2%	95.5%	61.7%	83.3%

2.4 Flux Calculation

With the efficiency determined, it is now possible to calculate the muon flux that passes though the detector. These calculations were made for both areas under consideration, using the equation:

$$\Phi_{muons} = \frac{n}{\varepsilon \, L \, A} \tag{5}$$

Where A is the area and L is the luminosity provided by the ATLAS experiment.

3 Simulation Analysis

The total received scoring plane of the simulation is 180x180cm^2, which is a much larger range than our detector (whose total area is only 30x30cm^2). For that reason, a cut had to be applied to limit the data analyzed to the area of interest. The cut on the domain can be visualized in fig. 11.

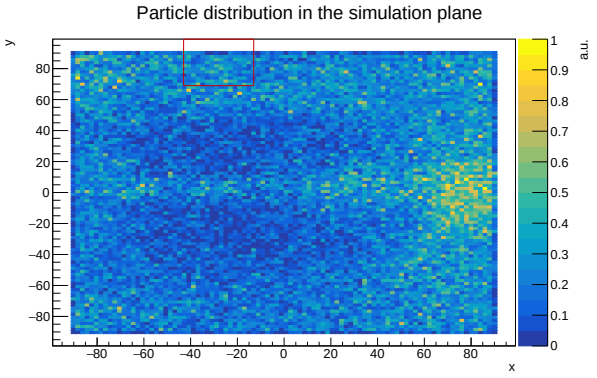

Figure 11: Distribution of data in the scoring plane, with detector delimitation (red square)

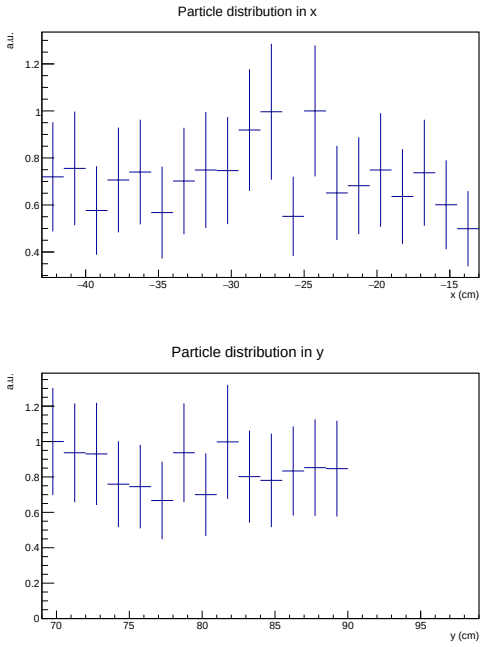

Figure 13. Distribution of data in the detector in x (top) and y (bottom)

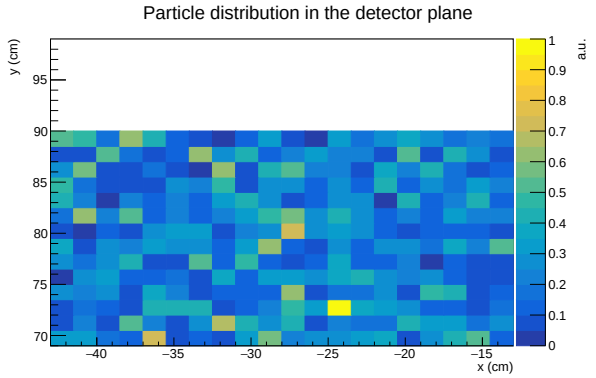

Figure 14: Distribution of data in the detector plane

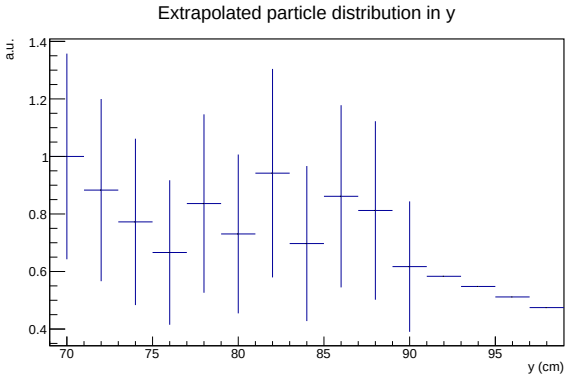

Figure 16: Y distribution fit

The cut demonstrates that there is a region of the detector which is unaccounted in the simulation, which can also be verified in the local distribution in the detector plane (figs. 13 and 14). There are two avenues by which to address this problem. Firstly, the calculation area can be restricted only to the section of the detector for which there is simulated data. Secondly, an extrapolation can be done to attempt to approximate the value for the simulation of the entire detector.

We considered both options, comparing the two results.

3.1 Extrapolation

The unaccounted section of the detector ranges from $y = 90$ to $y = 99$. To be able to do the extrapolation, therefore, the total distribution for the simulation in y had to be plotted. The graph obtained (fig. 15), shows several noteworthy structures, including a peak in the upper range of the domain. We decided to fit this peak as a gaussian, from where we obtained the following expression:

$$w(y) = (2.41 \pm 0.08)\exp\left(\frac{-[y - (74.21 \pm 2.07)]^2}{25.17 \pm 2.36}\right) \quad (6)$$

Using 6, we filled the remainder of the domain in y (fig. 16).

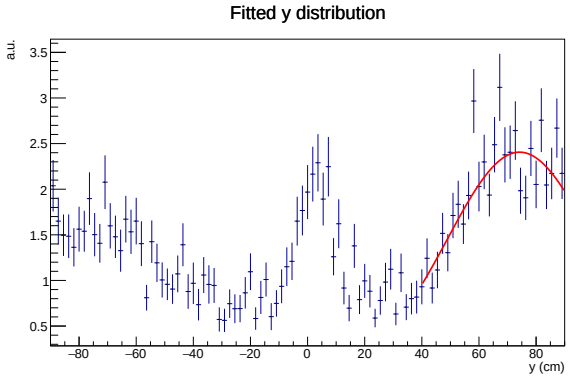

Figure 15: Y distribution fit

3.2 Flux calculation

To calculate the flux, the equation 5 was used. The N parameter is the total sum of the weights of the data points in the detector. The efficiency is not relevant in this calculation, as we are dealing with a simulation with no data loss. The luminosity was obtained from the number of simulated proton-proton collisions (N_{pp}) and the total inelastic cross-section for such collisions (σ_{inel}) through the formula:

$$L = \frac{N_{pp}}{\sigma_{inel}} \quad (7)$$

The values for the parameters for equation 7 are $N_{pp} = 2 \times 10^7$, and $\sigma_{inel} = (79.30.6)mb$. [3]

3.3 Particle type percentages

In order to characterize the particle makeup of our data, we calculated the percentage of muons and antimuons present. Without applying the weight, the number of events identified as muons (id=13) was considerably smaller than that of those identified as antimuons (id=-13): 78.29 % to 21.1 %. After applying the weight, this difference was reduced considerably, maintaining, however, a small leftover asymmetry: 51.9% to 48.1% .

We speculate that this is due to various factors, including production imbalances at the ATLAS collision site and effects from the LHC magnetic-fields.

4 Flux results

The calculated flux results are compiled in table 3.

Table 3: Flux values for different conditions

Flux($fb\ cm^{-2}$)	Cut area (30x21)	Full area (30x30)
Real flux	1.01×10^5	6.39×10^4
Simulated flux	$(1.7 \pm 0.05) \times 10^5$	$(1.51 \pm 0.05) \times 10^5$

We have obtained real results in the same order of magnitude as those obtained for the SND@LHC detector. [1]

However, there was significant difference in the values obtained for the real and simulated data, 136% for the entire area of the detector and 68% for the limited area, with the simulated flux's value being higher than the real.

These results suggest on one hand that the extrapolation made for the simulated data has a low accuracy, as it produces results more distant from the real data, and on the other hand that the simulated particles are overestimated. A higher predicted flux should be expected considering that the simulation used does not account for additional material traversed by the muons in the vicinity of the detector site. This may explain the overestimated flux obtained in simulation compared to the measurement made in data.

Acknowledgments

We thank our supervisors Cristóvão and Nuno for the opportunity to engage in this important work, and for the teachings this experience has provided.

References

[1] R. Albanese et al., *Measurement of the muon flux at the SND@LHC experiment*, Eur. Phys. J. C (2024) [https://doi.org/10.1140/epjc/s10052-023-12380-3]

[2] S. Navas et al. (Particle Data Group), Phys. Rev. D **110**, 030001 (2024) [https://doi.org/10.1103/PhysRevD.110.030001]

[3] T. Sýkora, *Total, elastic and inelastic p-p cross sections at the LHC*,https://indico.cern.ch/event/432527/contributions/1072410/attachments/1321213/1981420/xSections_ICHEP_2016_final_photosd.pdf (2016) [Online]